Lateral load bearing capacity of offshore high-piled wharf with batter piles

Yaofeng Xie[a,*], Chenglin Liu[a], Suyang Gao[a], Jieping Tang[b], Yan Chen[a]

[a] School of Transportation, Southeast University, China
[b] College of Geography and Marine Science, Nanjing University, China

ABSTRACT

Understanding the lateral load behavior of high-piled wharf is of practical value to structural design, and the horizontal load bearing capacity of the bent is essential to analyzing the behavior of the high-piled wharf. In this paper, finite element models of high-piled wharf are built in a general finite element software–ANSYS to investigate the lateral loading behavior. Parametric analyses have been performed on the working behavior of single pile with varying slopes and section sizes under different load levels. The behavior of bent with batter piles under different lateral loads is discussed. The formulas of lateral load vs. horizontal displacement for single pile and high-piled wharf are formulated and presented in this paper. The numerical simulation results of pile top displacement are found to be in good agreement with those predicted using the theoretical formula presented in this paper. These formulas, which describe the relationship between top displacement and stiffness, inclination and loads, can be useful to determine the horizontal load bearing capacity of the high-piled wharf with batter piles and can realize the real-time safety monitoring of the high-piled wharf for practical application.

1. Introduction

The high-piled wharf structures have been widely applied in ocean engineering and port engineering, evidenced by the many high-piled wharves constructed in the past three decades. The main loads on the high-piled wharf structures are horizontal loads caused by wave load, flow load, wind load and ship impact load (Zhu and Xie, 2015; Xie et al., 2015). While among these loads, the ship load should be the most emphasized for its largest magnitude, especially for the high-piled wharf located in the open sea.

Considering the fact that the lateral load capacity of plumb pile is limited, high-piled wharves with batter piles have been widely used in offshore structures in order to achieve improved lateral load capacity. However, with the development of larger size ships and increasing demand for safety, high-piled wharf is expected to sustain horizontal loads of greater magnitude. The deformation of the wharf structure subjected to horizontal loads has been a main concern to its safe operation and thus considered as an important engineering problem by engineers.

Previous studies on high-piled wharf have been mainly based on theoretical analysis, laboratory tests and the field experiment method. The underlying pile is an important foundation component in the high-piled wharf. The elastic theoretical method proposed by Poulos (1971) is one of the earliest methods for pile foundation analysis, in which the soil is assumed to be ideally homogeneous and isotropic in elastic half space. In the P-Y curve method proposed by Matlock (1970) (where P is the soil resistance along the pile, Y is the lateral deflection of the pile at the same location), the pile behavior under the lateral loads is described using a series of nonlinear curves regarded as the function of the depth along the pile, and also as the representative of the elastic-plastic analysis method. However, these theoretical analysis methods have limitation in practical application due to the complexity of the soil-pile interaction. Several researchers also conducted laboratory experiments and field tests on the high-piled wharf. Pan et al. (2000) studied the stress and the deformation of the pile under horizontal loading by doing scale model experiments. Bonakdar and Oumeraci (2015) conducted a small scale model tests in a 2 m-wide wave flume to investigate the pile group effect on the wave loading of a slender pile and tested different pile arrangement.

With advances in computing technology and finite element analysis software, numerical simulation based analysis methods have been widely employed, and potentially can be used to investigate the effect of a large number of influencing factors of the pile-supported platform under horizontal load. Additionally, numerical study is usually less costly and less time consuming than physical experiments even with small scale model.

Rajashree and Sitharam (2001) conducted finite element analysis of batter piles under lateral load by idealizing the piles as beam elements

and the soil as elastoplastic spring elements. The nonlinear soil behavior is represented by a hyperbolic relation. The importance of the degradation factor and its effect on the P-Y curves on batter piles are demonstrated.

With the widespread use of pile-supported platform in offshore structures, research works are also reported on the behavior of offshore high-piled wharf under horizontal load. Mostafa and Naggar (2004) studied the response of offshore platform subjected to extreme wave and current loading with varying parameter values. Giannakou et al. (2010) studied the seismic response of batter pile including the "kinematic" pile deformation as well as the "inertial" soil-pile-structure response using three-dimensional finite-element model in which elastic behavior was assumed for the soil, piles and the superstructure. Wang and He (2013) employed a 3-D elastic-plastic finite element model to analyze the load bearing capacity of vertical pile-supported wharf under horizontal loads with pseudo-static method. Fan and Yuan (2014) developed finite element models for ship-structure-soil inter-actions and identified four interaction phases for the overall flexural failure of the pile-supported platform as initial contact, unloading and free vibration and loading with approximate velocities. Muthukkumaran and Arun (2015) analyzed the soil-structure interac-tion behavior with varying seabed slope by performing static wave analysis on a typical fixed offshore platform using finite difference method. It is found that the lateral displacement at the pile top increases as the seabed slope increases.

Although the above literature review shows that a few factors have been considered such as the pile length, the stiffness of pile, the load inclination angle and the pile spacing of pile group, few researches on the displacement calculation method of the high-piled wharf under horizontal loads have been done. Therefore, it is of interest to carry out the research on the displacement calculation method for the high-piled wharf under horizontal loads. Theoretical research by Xie (1996) suggested that the problem of analyzing high-piled wharf can be resolved into analyzing bent structure. Determining the working properties of bent structure is the key component in studying the behavior of high-piled wharf.

In the present study, the finite element analysis software package-ANSYS is employed to simulate the deformation of high-piled wharf under the lateral load. The relationship between the lateral load and deformation is expatiated, and the theoretical formula is proposed. The field berthing test is used to investigate the theoretical formula. In this way, the lateral displacement under certain lateral load and the lateral bearing capacity under a limited displacement can be predicted.

2. Numerical model of high-piled wharf: description

2.1. Prototype of bent

As shown in Fig. 1, the section of the beam is an inverted "T" shape. The width of the lower rectangular beam section is 1.20 m, and its depth is 1.10 m. The width of the upper rectangular beam section measures 0.70 m, and its height measures 2.12 m. The base of the piles is assumed to be located at the same elevation. The section size of all the piles is equal to 0.6 m×0.6 m. The free length (i.e., length of the unburied part) of the piles in the vertical direction is 10 m. From left to right, the piles are labeled as #1 to #5 or from #1 to #9 respectively. The horizontal load is assumed to be a static concentrated load and is applied to the centroidal axis of the beam at one time for each loading case. The load direction is pointing to right. The parameters of the soil and the piles are shown in Tables 1, 2. Three different designs of the bent prototype models are showed in Fig. 2(a) to 2(c) respectively.

2.2. Basic assumption in the model

The following basic assumptions are made in the finite element model of the prototype high-piled wharf structures.
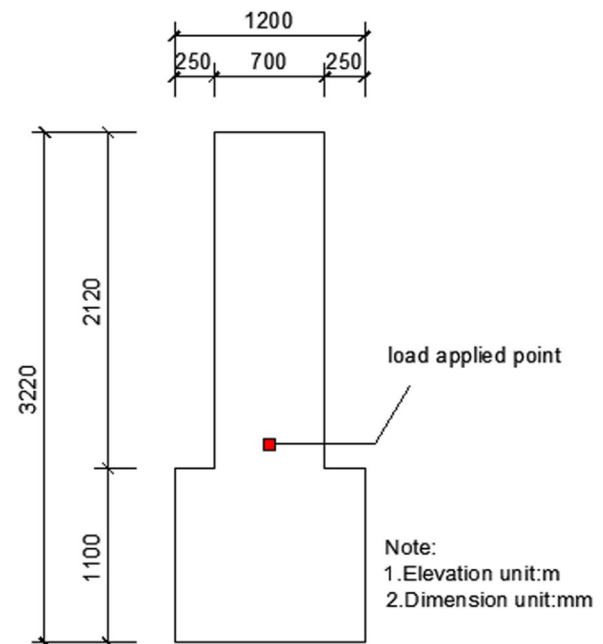

Fig. 1. The section of the beams.

(1) In the model, the soil is assumed to be continuous, homogeneous, and isotropic. The boundary conditions of the soil are given: the bottom surface of soil is constrained in all directions, and the side surfaces of soil are constrained in the horizontal directions.
(2) The elastic modulus and Poisson's ratio of the surrounding soil remain constant with the pile embedded in it.
(3) The pile and the soil are both assumed to behave as elastic-plastic material. The soil follows the Drucker-Prager Yield Criteria, which was also employed in previous study by Wang et al. (2014) as a classical model.
(4) Pile-soil interface is represented with a contact surface, and bottom section of the pile is laid on a horizontal surface.

2.3. Engineering parameters

The parameters of the soil and piles are listed in Tables 1 and 2, respectively. The parameters used for plastic soil behavior is material constant β and yield strength σ_y . $\beta = \frac{2sin\varnothing}{\sqrt{3}\,(3-sin\varnothing)}$, $\sigma_y = \frac{6ccos\varnothing}{\sqrt{3}\,(3-sin\varnothing)}$ (ANSYS Help version 16.0, 2014). Where $\varnothing$ refers to the internal friction angle, and c refers to the cohesion, the parameters $\varnothing$ and c are presented in Table 1.

The compressive strength of the concrete is C40. These engineering parameter values are taken from a real offshore pile-supported structure located in the Yangtze River estuary, China.

2.4. Contact surface setting

In the ANSYS model, the contact surface element is adopted to simulate the pile-soil interaction. In general, the following rules and some research experience are followed to define the target surface and contact surface between the piles and the soil,

(1) The fine mesh surface should be set as the contact surface, and the rough mesh surface should be set as the target surface.
(2) The flat and concave surface should be set as the target surface.
(3) The harder one should be set as the target surface, and the softer one should be set as the contact surface.
(4) The surface with higher order element as base elements should be set as the contact surface, and the surface with lower order element should be set as the target surface.

Table 1
The parameters of soil.

Material	Density (kg/m^3)	Elastic modulus (Mpa)	Poisson's ratio	Cohesion (kPa)	Internal friction angle (°)	Expansion angle (°)
Soil	1950	8.6	0.3	9	33	30

(5) The larger surface should be set as target surface, and the smaller surface should be set as contact surface.

(6) The nodes belonging to both contact surfaces are not required to be corresponding to each other, but more accurate results can be obtained if they are corresponding to each other.

(7) The continuity of the main surface should be ensured.

(8) The normal directions of a pair of surfaces should be opposite to each other.

(9) The surface with larger stiffness should be the main surface.

In the ANSYS software package, Conta 174 is an 8-node element that is generally used for rigid-flexible and flexible-flexible contact analysis and is applicable for 3-D geometries. Targe 170 is intended to represent 3-D target surfaces for the associated contact elements (e.g. Conta 174). To create the "contact-target pair", the pile is selected as the target surface and the target segment element Targe 170 is used to overlay the pile body. Correspondingly, the soil is set as the subordinate contact surface and the surface-to-surface contact element Conta 174 is used to overlay the soil surface which is associated with the pile body in the present finite element analysis (ANSYS Help version 16.0, 2014).

The node pairs of the discrete element built on the contact surfaces should satisfy the displacement compatibility condition and the Hooke's Law. The soil and the piles cannot penetrate into each other. The pressure is the only normal force, and the friction force is the only tangential force between the soil and piles. The friction coefficient is taken as 0.2.

3. Finite element modeling of single pile

3.1. Model details

Finite element models of a single pile with different slopes and subjected to different loads were built in ANSYS. The slopes of the batter piles are chosen as 1:7, 1:6, 1:5, 1:4 and 1:3 respectively. The horizontal load is applied to the top end of the pile. The bases of the piles are all located at the same elevation level. The free length of the piles in the vertical direction is 10 m. The elastic modulus and Poisson's ratio are given in Table 2. By comparing the results from model simulation results, the relationships between the displacement and slope, load and stiffness can be established for the piles.

3.2. Finite element model analyses

The bottom and surroundings of the soil body are set as fixed constraints. The displacements of the plumb pile and the batter pile are obtained when applying different loads to the piles separately.

In this part, in order to understand the relationship between the displacements of piles and different slopes and stiffness, the pile sections are set to be 0.4 m×0.4 m, 0.6 m×0.6 m, 0.8 m×0.8 m, 1.0 m×1.0 m, respectively; other pile parameters besides the pile

sections are the same as those listed in Table 2. The displacements of the piles with different slopes and stiffness subjected to different loads recorded from finite element analysis results are listed in Tables 3–5.

3.3. Behavior analysis of single pile

3.3.1. Relationship between top displacement and slope of single pile

It is found that the relationship between the horizontal displacement of the pile top and the pile inclination to the power of m is almost linear, as shown in Fig. 3. The least square method is adopted to fit the computed data.

Eq. (1) can be expressed as below,

$$y_s = (1 + \alpha^m)y_0 \qquad (1)$$

where y_s is the horizontal displacement of single pile top (unit = m), α is the inclination angle between pile longitudinal axis and vertical direction (unit = radian), y_0 is the horizontal displacement of the plumb pile top under identical load (unit = m), and m is the exponent that is related to the inclination angle (Generally, it varies from 1.3 to 1.5.).

3.3.2. Top displacements of single plumb pile

The plumb pile inserted in the soil is similar to a cantilever beam structure. Therefore, it is reasonable to assume that the top horizontal displacement of the plumb pile is inversely proportional to its stiffness while the top displacement is proportional to its free length cubed. Eq. (2) below can be written out for the top force-displacement of the plumb pile,

$$y_0 = (l_0 + l_q)^3 Ft/(3EI) \qquad (2)$$

where Ft is the horizontal load acting on the pile top (unit: kN), l_0 is the free length of the pile in vertical direction (unit: m), l_q is the distance between the embedded point (all piles are assumed to be embedded at their maximum moment points) and the soil surface (unit: m), and EI is the flexural stiffness of the pile (unit: $kN{\cdot}m^2$).

$$l_q = (6 + 0.016Ft)b \qquad (3)$$

Where b is the width of the square-section pile (unit: m).

Fig. 4 shows the relationship between the flexibility (inverse of the stiffness) and the top horizontal displacement of the plumb pile. The curves are seen to match very well with those predicted by Eq. (2).

In Eq. (2), y_0 is expressed as a function of the flexural stiffness of the pile, the property of the soil and the load. The embedded depth is greater when the load is larger. Further research may be needed if other factors are to be taken into account in this formula.

By combing the above equations, the top force vs. displacement relationship of single pile can be derived as Eq. (4) below,

$$y_s = (1 + \alpha^m)(l_0 + l_q)^3 Ft/(3EI) \qquad (4)$$

Fig. 5 shows the results of the theoretical calculation and numerical

Table 2
The parameters of piles.

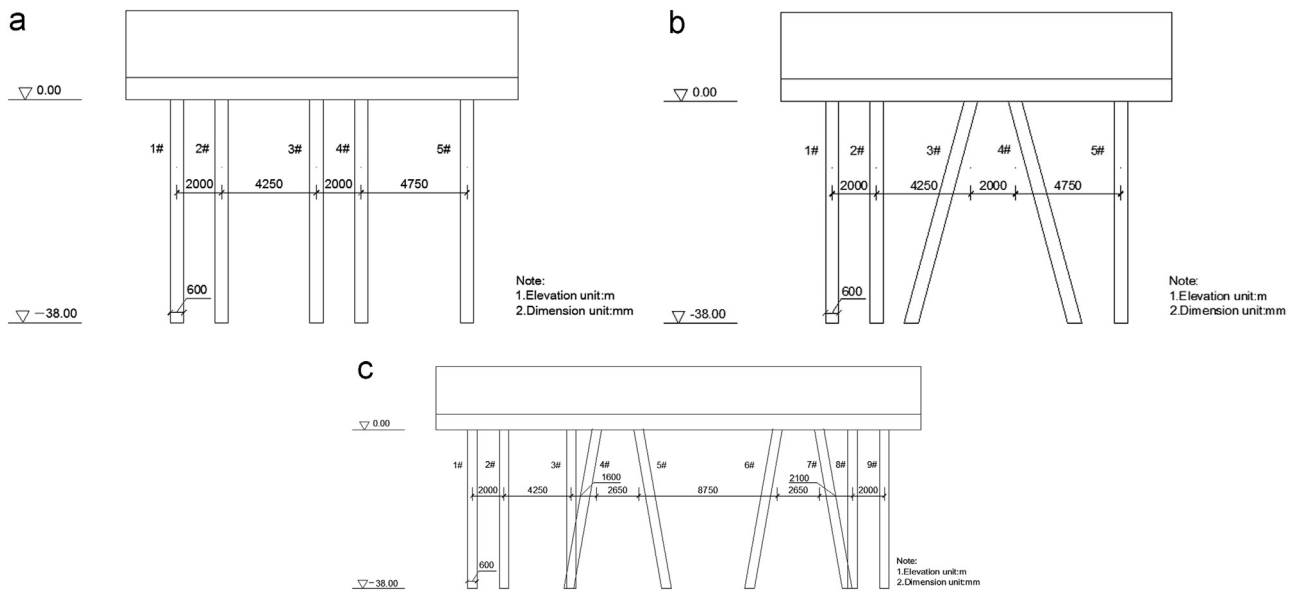| Material	Section Size (m)	Elastic modulus (Mpa)	Yield Stress (Mpa)	Moment of Inertia (m^4)	Poisson's ratio	Length (m)	Buried depth (m)
Plumb pile	0.6×0.6	3.25×10⁴	65	0.0108	0.2	38	28
Batter pile(1:5)	0.6×0.6	3.25×10⁴	65	0.0108	0.2	38.8	28.6

Fig. 2. Bent structure layout and dimensions. (a). Layout of bent structure with all plumb piles. (b). Layout of bent structure with one pair of batter piles. (c). Layout of bent structure with two pairs of batter piles.

Table 3
Horizontal displacements of single pile with different stiffness under 5 kN load.

Stiffness EI ($kN \cdot m^2$)	Pile section ($m \times m$)	Horizontal displacement of pile top (m)					
		Plumb pile	Batter pile (1:7)	Batter pile (1:6)	Batter pile (1:5)	Batter pile (1:4)	Batter pile (1:3)
69,333.33	0.4×0.4	4.68 E−02	4.87E−02	4.92E−02	5.05E−02	5.27E−02	5.68E−02
351,000	0.6×0.6	1.20E−02	1.25E−02	1.27E−02	1.29E−02	1.34E−02	1.45E−02
1,109,333	0.8×0.8	4.88E−03	5.12E−03	5.17E−03	5.28E−03	5.45E−03	5.85E−03
2,708,333	1.0×1.0	2.52E−03	2.64E−03	2.67E−03	2.73E−03	2.83E−03	3.02E−03

Table 4
Horizontal displacements of single pile with different stiffness under 10 kN load.

Stiffness EI ($kN \cdot m^2$)	Pile section ($m \times m$)	Horizontal displacement of pile top (m)					
		Plumb pile	Batter pile (1:7)	Batter pile (1:6)	Batter pile (1:5)	Batter pile (1:4)	Batter pile (1:3)
69,333.33	0.4×0.4	9.54 E−02	9.97 E−02	1.01 E−01	1.03 E−01	1.08 E−01	1.17 E−01
351,000	0.6×0.6	2.42 E−02	2.54 E−02	2.56 E−02	2.62 E−02	2.72 E−02	2.95 E−02
1,109,333	0.8×0.8	9.77 E−03	1.02 E−02	1.03 E−02	1.06 E−02	1.09 E−02	1.17 E−02
2,708,333	1.0×1.0	5.05 E−03	5.28 E−03	5.35 E−03	5.46 E−03	5.65 E−03	6.03 E−03

Table 5
Horizontal displacements of single pile with different stiffness under 50 kN load.

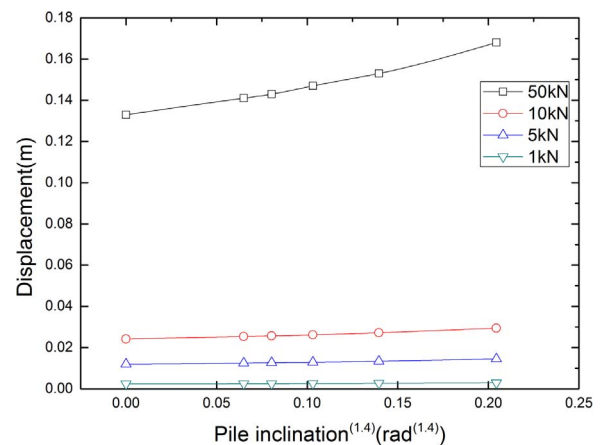| Stiffness EI ($kN \cdot m^2$)	Pile section ($m \times m$)	Horizontal displacement of pile top (m)					
		Plumb pile	Batter pile (1:7)	Batter pile (1:6)	Batter pile (1:5)	Batter pile (1:4)	Batter pile (1:3)
351,000	0.6×0.6	1.33 E−01	1.41 E−01	1.43 E−01	1.47 E−01	1.53 E−01	1.68 E−01
1,109,333	0.8×0.8	5.11 E−02	5.40 E−02	5.49 E−02	5.59 E−02	5.82 E−02	6.29 E−02
2,708,333	1.0×1.0	2.59 E−02	2.72 E−02	2.76 E−02	2.83 E−02	2.93 E−02	3.15 E−02

Fig. 3. Displacement of pile top vs. pile inclination angle. (The exponent m here is equal to 1.4).

4. Finite element analysis of pile-supported bent with batter piles

4.1. FE model and FEA results of bent with plumb piles

4.1.1. Model description of bent with plumb piles

There are 5 piles total in the bent model, and these 5 piles are all plumb piles. In the bent, the spacing between the piles is 2 m, 4.25 m,
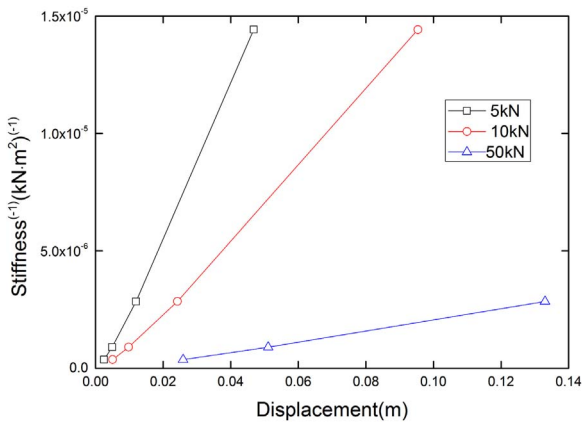
simulation. In Fig. 5(a), the size of the pile is $0.6 m \times 0.6 m$. In Fig. 5(b), the size of the pile is $0.8 m \times 0.8 m$. In Fig. 5(c), the size of the pile is $1.0 m \times 1.0 m$. As can be seen from Fig. 3, the results of the theoretical calculation match well with the data from the numerical model study. Fig. 6 shows the lateral load-displacement relation for single pile with various pile slope, and the pile section is $0.6 m \times 0.6 m$.

Fig. 4. The relationship between the stiffness and the horizontal displacement of plumb pile.
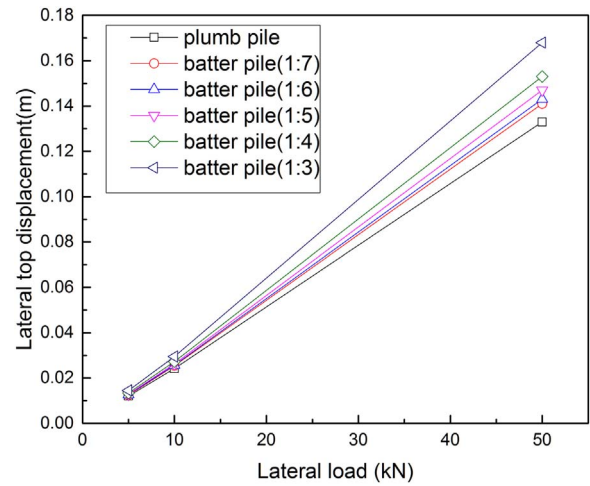

Fig. 6. Lateral load-displacement relation for single pile with varying slope.

2 m, and 4.75 m respectively from left to right (see Fig. 2(a)). The pile section is set to be $0.6m \times 0.6m$.

For the finite element modeling of the entire structure in ANSYS, tetrahedron element is adopted to mesh the structure model. In particular, for the bent structure, 10-nodes tetrahedron solid element (solid 187) is employed for meshing, while for the soil part, 10-nodes tetrahedron solid element (solid 92) is utilized. The solid 92 element is a 3-D, 10-node element having three degrees of freedom at each node. It has a quadratic displacement behavior and has capabilities of plasticity, creep, stress stiffening, large deflection and large strain.

The solid 187 element is a higher 3-D, 10-node element, covering all the capabilities that solid 92 element has. Fig. 7(a) shows the finite element model of the pile-bent structure with meshing. Contact surface element is used to simulate the pile-soil interactions. Fig. 7(b) shows the geometry of solid elements and contact surface elements.

Based on the finite element analysis results, the horizontal displacement of the piles of bent with all plumb piles under different horizontal loads applied to the centroidal axis of the beam are given in Table 6.
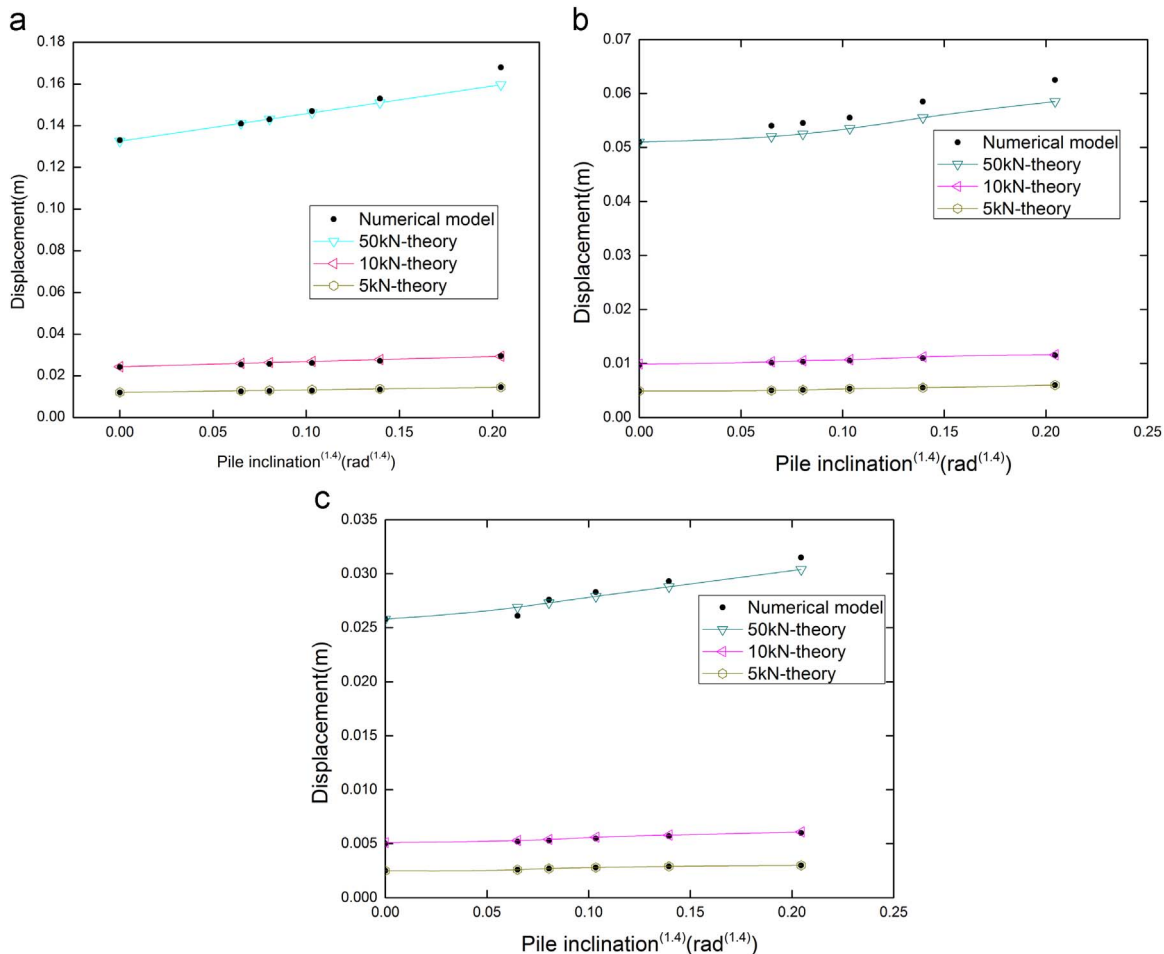

Fig. 5. Comparison of theoretical calculation and numerical simulation results. (a) Pile with square section of 0.6 m×0.6 m. (b) Pile with square section of 0.8 m×0.8 m. (c) Pile with square section of 1.0 m×1.0 m.
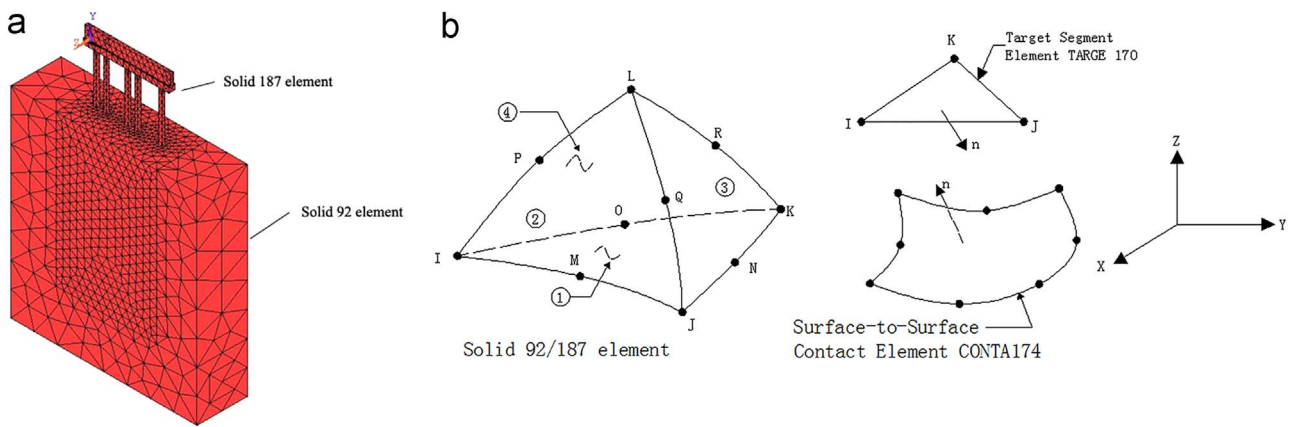
Fig. 7. (a) Element division of bent with all plumb piles. (b) Geometry of solid elements and contact surface elements.

4.1.2. Displacement of bent with plumb piles

Fig. 8(a) and Fig. 8(b) show the displacement profiles along the length of pile #1 and pile #3 in the bent with all plumb piles under different horizontal loads respectively. Fig. 9 presents the lateral load-displacement relation of bent with plumb piles.

It is shown in this study that under the same load, pile-top displacements of each pile are basically the same and under different loads, the displacements of each pile all decrease to zero at the section 15-m down from the pile top.

4.2. FE model and FEA results of bent with a pair of batter piles

4.2.1. Model description of bent with a pair of batter piles

The finite element model of the bent includes five piles including a pair of batter piles with a slope of 1:5. In the bent with batter piles, the spacing between each pile are 2 m , 4.25 m , 2 m, and 4.75 m at top (see Fig. 2(b)). The pile section is set to be $0.6m \times 0.6m$.

In the finite element model of the bent, the structure element, the contact surface element and other related settings are identical to those in the finite element model of the bent with all plumb piles. Fig. 10 shows the element division of the bent model.

4.2.2. Displacement of bent with a pair of batter piles

The lateral load is applied to the centroidal axis of the beam. From the finite element simulation results, it is seen that the top displacements of all piles in the bent are the same in the horizontal direction at all load levels. Table 7 lists the top displacements of the bent.

This study shows that: (1) At the same load level, pile-top displacements of all piles are basically the same; (2) Under different load levels, the displacements of the three plumb piles all decrease to zero at locations 15-m away from the pile top; (3) The displacement of batter pile #3 changes from positive to negative values more quickly than those of plumb piles; (4) The displacement of batter pile #4 does not switch direction along its length.

Fig. 11(a) and Fig. 11(b) show the distribution profile of the displacement responses along pile #1 and pile #3 of the bent with a

pair of batter piles in vertical direction under different horizontal load levels respectively. Fig. 12 illustrates the lateral load-displacement relation of bent with a pair of batter piles.

4.3. FE model and FEA results of bent with two pairs of batter piles

4.3.1. Model description of bent with two pairs of batter piles

The finite element model of the bent is composed of nine piles including two pairs of batter piles with a slope of 1:5. In the bent, the spacing between each pile are 2 m, 4.25 m, 1.6 m, 2.65 m, 8.75 m, 2.65 m, 2.1 m, and 2 m from left to right pile top respectively (Fig. 2(c)). The pile section is set to be $0.6m \times 0.6m$.

In the finite element model of the bent, the structure element, the contact surface element and other related settings are identical to those in the finite element model of the bent with all plumb piles. Fig. 13 shows the element division of the bent model.

4.3.2. Displacement of bent with two pairs of batter piles

The lateral load is applied to the centroidal axis of the beam. The pile top displacement of bent with two pairs of batter piles are presented in Table 8.

This study shows that: (1) At the same load level, pile-top displacements of all piles are basically the same; (2) Under different load levels, the displacements of the four plumb piles all decrease to zero at locations 15-m away from the pile top; (3) Because batter pile #4 and batter pile #6 are under tension, the displacements of the lower half of these two piles keep as negative, and the smaller the load is, the closer the zero displacement point is to pile top; (4) Because pile #5 and pile #7 are under compression, the displacements of these two piles remain in the positive direction along its length.

Fig. 14(a) to 14(c) show the distribution profile of the displacement responses along pile #1, pile #4 and pile #6 of the bent with two pairs of batter piles under different horizontal load levels respectively. Fig. 15 presents the lateral load-displacement relation for bent with two pairs of batter piles.

Table 6
Horizontal displacement of the piles of bent with all plumb piles.

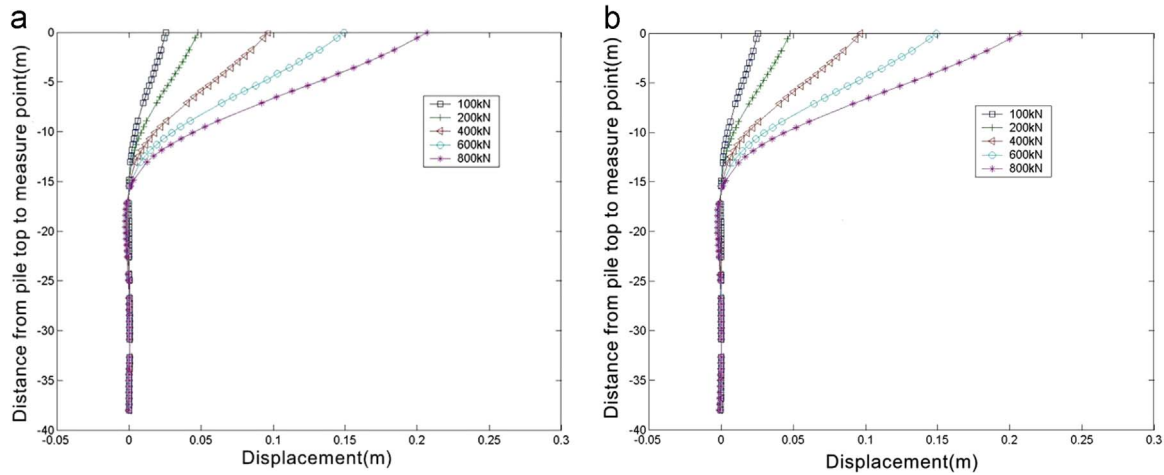| Load (kN)	Displacement of pile at soil surface (m)					Pile top displacement (m)
	Pile #1	Pile #2	Pile #3	Pile #4	Pile #5	
100	3.91E−03	3.95E−03	4.02E−03	3.92E−03	3.62E−03	2.55E−02
200	7.95E−03	7.93E−03	8.13E−03	7.87E−03	7.31E−03	4.75E−02
400	1.76E−02	1.72E−02	1.77E−02	1.71E−02	1.59E−02	9.64E−02
600	2.96E−02	2.84E−02	2.94E−02	2.80E−02	2.60E−02	1.49E−01
800	4.37E−02	4.17E−02	4.31E−02	4.08E−02	3.76E−02	2.07E−01

Fig. 8. Displacement profiles of Piles #1 and #3 subjected to lateral load. (a) Pile #1 of bent with all plumb piles. (b) Pile #3 of bent with all plumb piles.
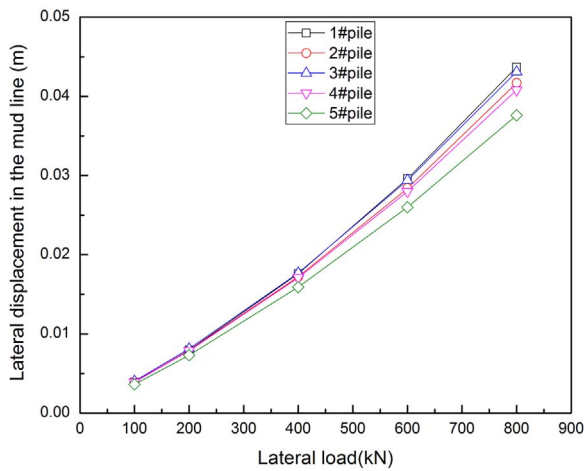

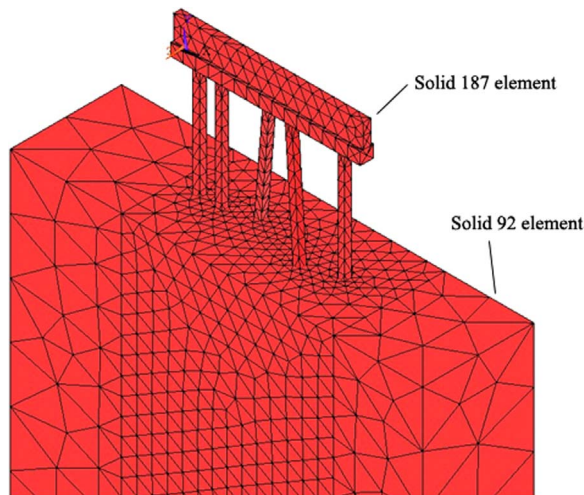**Fig. 9.** Lateral load-displacement relation of bent with all plumb piles.

Fig. 10. Meshed finite element model of the bent structure with a pair of batter piles.

4.4. Pile group coefficients of high-piled wharf

Based on the result of numerical simulation and analytical study, the displacement at the top section of each pile are found to be almost the same. Considering that the minimum pile space is larger than 3 times of pile section, which has little influence on the pile interaction. The pile group coefficient is regarded to be merely related to the number of piles from the view of engineering practice. The pile group coefficients formula can be expressed as follows:

For vertical high-piled wharf:

$$\eta_1 = n_1^{0.99} \tag{5}$$

For high-piled wharf with batter piles:

$$\eta_1 = n_1^{0.99} n_2^{0.22} \tag{6}$$

And the pile group coefficients of the soil surface can be expressed as:

$$\eta_2 = 1.0{\sim}1.2 \tag{7}$$

where η_1 is the pile group coefficients of pile top; η_2 is the pile group coefficients of soil surface; n_1 and n_2 are total numbers of plumb piles and batter piles respectively.

5. Load vs. displacement relationship of high-piled wharf with batter piles

Based on the data from the afore-mentioned finite element simulation study, the relationship of lateral load and bent displacement can be established and presented in this section. The bent top displacement is comprised of two parts: pile displacement at the soil surface section, w_h, and the deformation of the pile portion above the soil surface, w_d. Combined with theoretical analysis presented below, pile-top displacement formula can be derived. The following assumptions are made in the formulation presented here: (1) pile top's horizontal displacements are uniform along the wharf platform beam; (2) horizontal force is transmitted along the beam, and then to the piles.

Free body diagram of the beam and piles above the soil surface is schematically shown in Fig. 16. Fig. 16 illustrates the process of solving the high-piled wharf with batter piles using displacement method in structural mechanics. Generally, F is lateral load acting on the beam, F_i'

Table 7
Pile top horizontal displacement of the bent with a pair of batter piles.

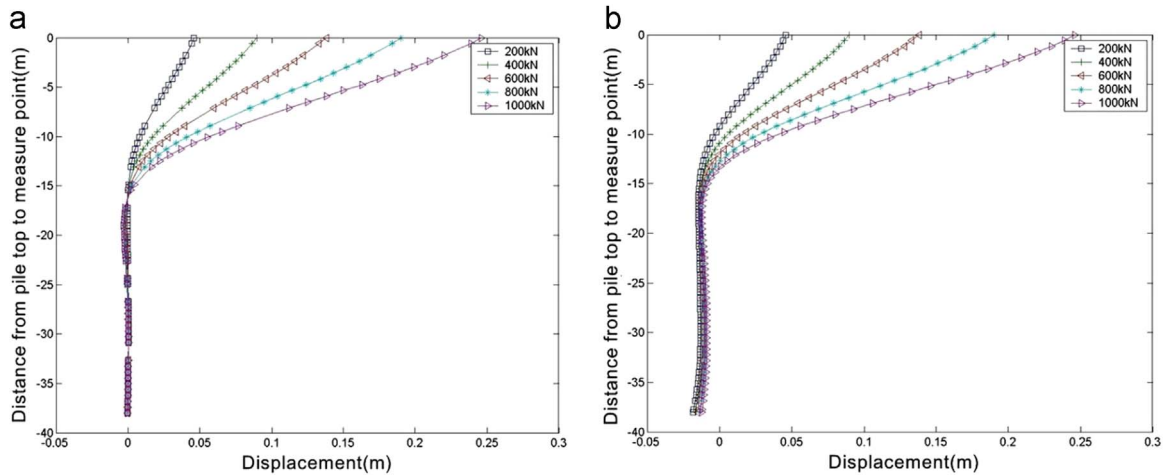| Load (*kN*)	100	200	400	600	800	1000
Displacement (*m*)	2.06E−02	4.57E−02	8.95E−02	1.38E−01	1.90E−01	2.46E−01

Fig. 11. The distribution law of displacements along piles in vertical direction. (a) Pile #1 of bent with a pair of batter piles. (b) Pile #3 of bent with a pair of batter piles.
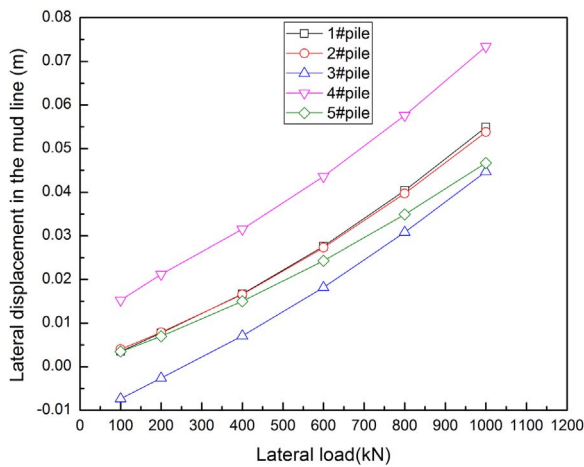

Fig. 12. Lateral load-displacement relation of bent with a pair of batter piles.
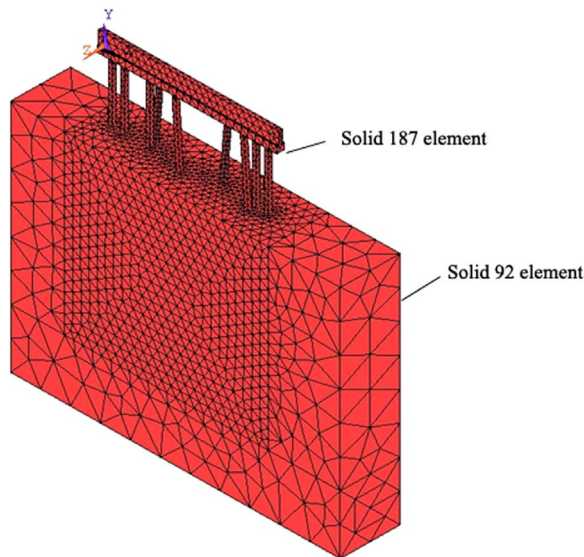

Fig. 13. Meshed finite element model of the bent structure with two pairs of batter piles.

is the shear force acted on the pile head while the F_i is the shear force acting on the beam, whose value is equal to F_i'. The lower end sections of all piles are assumed to be embedded at their maximum moment points, and rigid connection assumption is adopted for the connection of the upper pile end section and beam (for the sake of showing internal

Table 8
Pile top horizontal displacement of the bent with two pairs of batter piles.

Load (kN)	200	400	600	800	100	1400	1600	2000
Displacement (m)	1.64 E–02	3.47 E–02	5.40 E–02	7.44 E–02	9.6 E–02	1.43 E–02	1.68 E–01	2.24 E–01

forces, the piles are drawn separately from the beam at the section cut). From basic structural mechanics theory, the pile top displacement formula can be derived as below,

$$w_d = w_i = (F_i l^3/12EI\cos^3\alpha_i)\cos^2\alpha_i + (F_i l/EA\cos\alpha_i)\sin^2\alpha_i \qquad (8)$$

where i denotes the ith pile. α_i is the inclination angle between ith pile longitudinal axis and vertical direction, as shown in Fig. 16. According to the Newton's third law, the total force acting on the beam F is equal to the forces contributed by all connecting piles,

$$F = \sum_{i=1}^{i=n} F_i = \sum_{i=1}^{i=n} \frac{w_i}{\frac{l^3}{12EI\cos\alpha_i} + \frac{l\sin^2\alpha_i}{EA\cos\alpha_i}} \qquad (9)$$

Because the pile top displacements are the same, and if the slope of all batter piles is assumed to be constant, the following formula can be written out for the displacement of pile above soil surface,

$$w_d = \frac{\eta_1 F}{EI\cos\alpha\left[\frac{12n_1}{l^3} + \frac{12n_2}{l^3 + 12l(I/A)\sin^2\alpha}\right]} \qquad (10)$$

According to the data of plumb pile at soil surface from the FE simulation study, the pile's horizontal displacement at soil surface section can be expressed as,

$$w_h = \frac{\eta_2}{n_1 + n_2\left(\frac{1}{\cos\alpha} + \frac{12I\sin^2\alpha}{Al^2\cos\alpha}\right)} \frac{Fl^2}{5kEI} \qquad (11)$$

Combining Eq. (10) with Eq. (11), the total pile top displacement can be written as,

$$w = w_d + w_h = \frac{\eta_1 F}{EI\cos\alpha\left[\frac{12n_1}{l^3} + \frac{12n_2}{l^3 + 12l(I/A)\sin^2\alpha}\right]} + \frac{\eta_2}{n_1 + n_2\left(\frac{1}{\cos\alpha} + \frac{12I\sin^2\alpha}{Al^2\cos\alpha}\right)}$$

$$\frac{Fl^2}{5kEI} \qquad (12)$$

where w is the pile top displacement, w_d is the pile top displacement due to the deformation of the segment above the soil surface, w_h is the pile top displacement at soil surface, η_1, η_2, n_1 and n_2 can be referred to
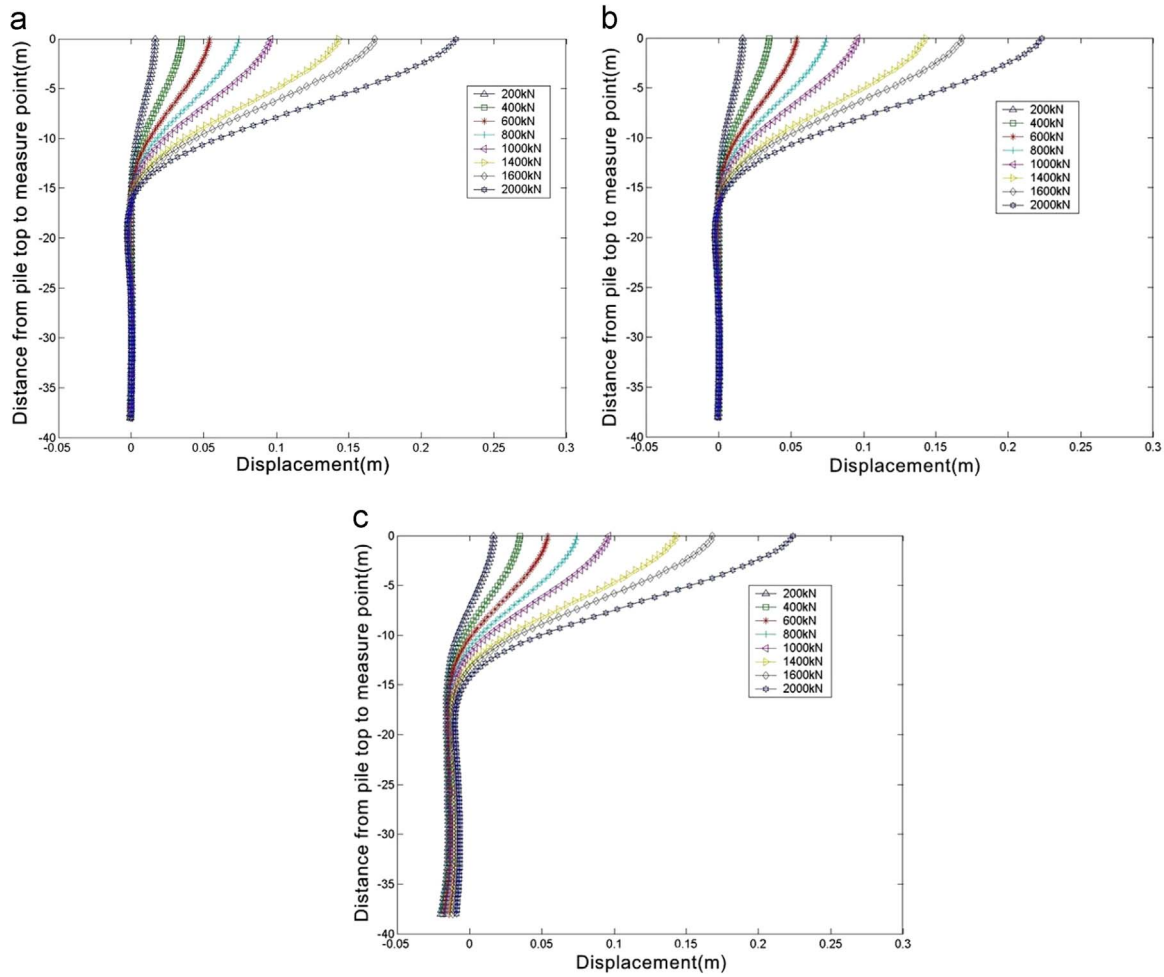
Fig. 14. Distribution profile of horizontal displacements along piles. (a) Pile #1 of bent with two pairs of batter piles. (b) Pile #4 of bent with two pairs of batter piles. (c)Pile #6 of bent with two pairs of batter piles.
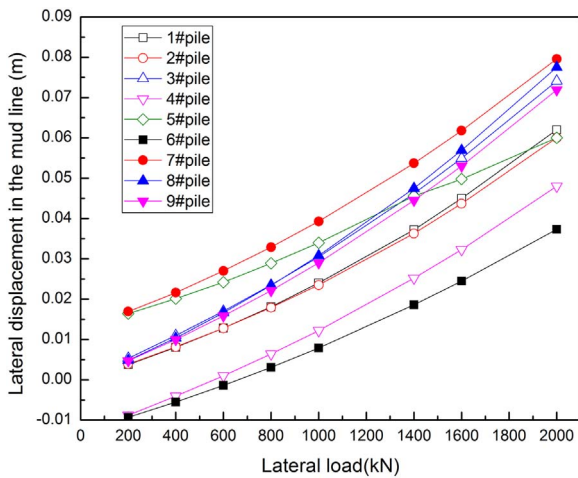

Fig. 15. Lateral load-displacement relation for bent with two pairs of batter piles.

Fig. 16. Free body diagram of bent model.

Eqs. (5) to (7), α is the slope of batter pile, E is the modulus of elasticity of pile material, I is the moment of inertia of the pile's section, k is the pile deformation coefficient($k = \sqrt{\frac{m_1 b_1}{EI}}$, m_1 is the horizontal resistance coefficient of foundation soils), b_1 is the pile calculation width ($b_1 = K_f \cdot K_0 \cdot K \cdot b$), b is the pile section width, K_f is the property conversion coefficient ($K_f = 1.0$), K_0 is the force conversion coefficient ($K_0 = 1 + 1/b$), and K is the pile influence coefficient($K = 1.0$). l is distance from the pile top section to maximum moment point along
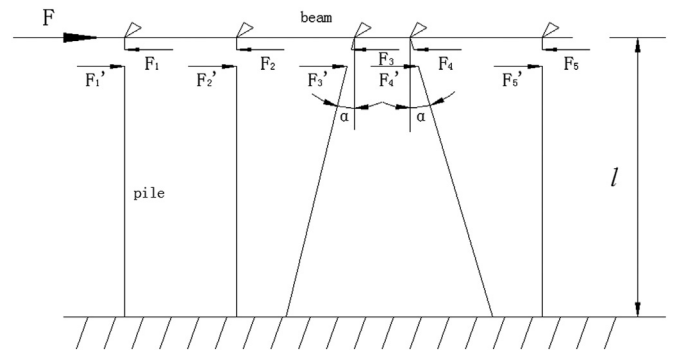
pile body in vertical direction ($l = l_0 + l_q$), l_0 is the distance from the pile top to soil surface in vertical direction, l_q is the distance between the embedded point.

Based on the above formulation, Eq. (12) can be used to determine the pile top force-displacement relationship. Table 9 shows the results of both numerical simulation study and the results predicted using Eq. (12).

In order to verify the finite element model and theoretical formula, a berthing test for high-pile wharf was conducted. The experimental test site is located in the middle and lower reaches of the Yangtze River. The high-pile wharf measures 700 $m \times 300$ m, comprising of eleven segmentations. The berthing test was focused on the seventh segmen-

Table 9
Comparison of pile top displacement from numerical simulation and Eq. (12).

| Load (*kN*)	Top displacement from FE simulation (*m*)			Top displacement From Eq. (12) (*m*)		
	Plumb pile bent	One batter pile bent	Two batter piles bent	Plumb pile bent	One batter pile bent	Two batter piles bent
200	4.75E−02	4.57E−02	1.64E−02	3.99E−02	3.60E−02	1.75E−02
400	9.64E−02	8.95E−02	3.47E−02	7.98E−02	7.20E−02	3.49E−02
600	1.49E−01	1.38E−01	5.40E−02	1.20E−01	1.08E−01	5.24E−02
800	2.07E−01	1.90E−01	7.44E−02	1.60E−01	1.44E−01	6.99E−02
1000		2.46E−01	9.60E−02		1.80E−01	8.74E−02
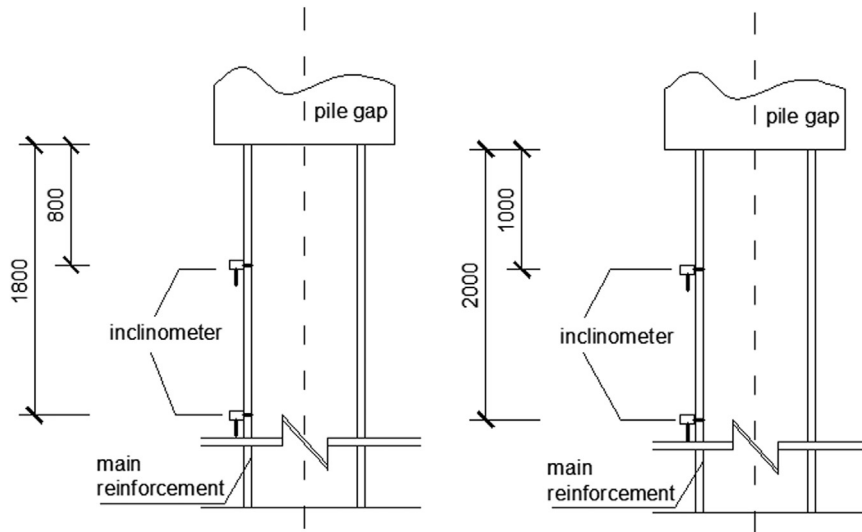
Fig. 17. Arrangement of inclinometers along the pile body (unit: mm).

tation. The bent is composed of nine piles including two pairs of batter piles with a slope of 1:5. In the bent, the spacing between each pile are 2 *m*, 4.25 *m*, 1.6 *m*, 2.65 *m*, 8.75 *m*, 2.65 *m*, 2.1 *m*, and 2 *m* from left to right pile top, respectively. The pile section is 0.6 *m*×0.6 *m*, as shown in Fig. 2(c).

The field test data was collected from the 'Youmei' Ship (the ship gross tonnage is 36,498 t) berthing test, in which force of the rubber fender and displacement of the bent were measured in separate berthing test (JPWTRCET, 2012). In berthing test, the ship gross tonnage is calculated by measuring waterline depth, and the speed and angle of ship berthing were obtained from GPS data. The locations of the inclinometers along the pile body are shown in Fig. 17.

Fig. 18 shows the comparison of results from numerical simulation study, theoretical formula (Eq. (12)) and experimental data (berthing

test). As is shown in Fig. 18, the results from the numerical simulation study and those predicted by the theoretical formula are close to the three berthing test data points. It should be noted that the berthing test only involved load amplitude lower than 450 kN. If the force further increases, the results given by the theoretical formula are slightly higher than the numerical simulation results. This clearly shows that Eq. (12) can be used to estimate the bearing capacity of the bent.

The bent structure is the basic structure of a high-piled wharf. Previous research has shown that the calculation formulas for high-piled wharf can be extended to those for the bent structure in ocean engineering and port engineering. Eq. (12) is capable of estimating the bearing capacity of the high-piled wharf with batter piles.

6. Conclusions

To study the working behavior of offshore high-piled wharf under lateral loading, finite element models of single pile and high-piled wharf are built in a general finite element analysis software – ANSYS. Parameters including the slopes, section sizes of the piles, and lateral load magnitude were taken into account for single pile analysis. The slopes of the batter piles were 1:7, 1:6, 1:5, 1:4, and 1:3, respectively. Pile-soil interface is modeled with the contact surface element in ANSYS. The behavior of bent structure with batter piles under different lateral loads is discussed. Based on the analysis results from the models considered in this study, the following conclusions can be drawn.

(1) The top displacement of the plumb pile is almost linearly proportional to the horizontal load under allowable working conditions.
(2) The single pile force vs. displacement formula and high-piled wharf force vs. displacement formula are presented based on the results in the present study. Through comparing the results from the simulation results and berthing test results with theoretical
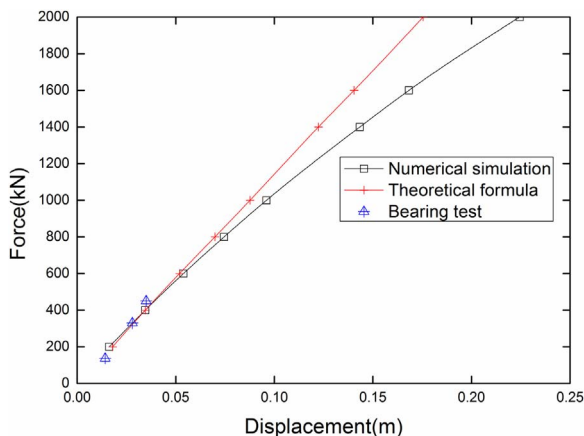

Fig. 18. Comparison of numerical simulation, theoretical formula and experimental (berthing test) results.

formula, Eq. (12) is shown to be reasonably accurate when the load amplitude is lower than 450 kN. This formula is of practical value to offshore platform structure designs.

(3) Considering that the allowable lateral displacement of high piled wharf is limited in a certain range, as well as the lateral force. The lateral load acting on the high-piled wharf can be obtained through the Eq. (12) if the lateral displacement of the high-piled wharf is provided. Or to get the lateral displacement according to the lateral load through Eq. (12). For practical application, according to the force vs. displacement relationship, the real-time monitoring can be realized.

(4) It should also be noted that the Eq.(12) is specific for the soil mechanical properties and pile parameters analyzed in this paper and should be cautious when applied to other situations.

The analysis of high-piled wharf can be extended to the bent structure in ocean engineering and port engineering, and the force vs. displacement relationship of the bent structure is thus a key research topic.

References

Ansys Help, 2014. version16.0. Ansys Inc.,

Bonakdar, L., Oumeraci, H., 2015. Pile group effect on the wave loading of a slender pile: a small-scale model study. Ocean Eng. 108, 449–461.

Fan, W., Yuan, W.C., 2014. Numerical simulation and analytical modeling of pile-supported structures subjected to ship collisions including soil-structure interaction. Ocean Eng. 91, 11–27.

Giannakou, A., Gerolymos, N., Gazetas, G., et al., 2010. Seismic behavior of batter piles: elastic response. J. Geotech. Geoenviron. Eng. 136 (9), 1187–1199.

Jiangsu provincial water transport research center of engineering technology (JPWTRCET), 2012. The report on deformation characteristics of high-pile pier structure under berthing load.

Matlock, H., 1970. Correlations for design of laterally loaded piles in soft clays. In: Proceedings of the 2nd Annual Offshore Technology Conference. OTC, Vol.1, pp. 577–594.

Mostafa, Y.E., Naggar, M.H.E., 2004. Response of fixed offshore platforms to wave and current loading including soil–structure interaction. Soil Dyn. Earthq. Eng. 24, 357–368.

Muthukkumaran, K., Arun, K.S., 2015. Erratum to: Effect of seabed slope on the pile behaviour of a fixed offshore platform under lateral forces. J. Ocean Eng. Mar. Energy 1 (3), 223–236.

Pan, J., Goh, A., Wong, K., Teh, C., 2000. Model tests on single piles in soft clay. Can. Geotech. J. 37 (4), 890–897.

Poulos, H.G., 1971. Behavior of laterally loaded piles: I-single piles. J. Soil Mech. Found. Div. 97 (5), 711–731.

Rajashree, S., Sitharam, T., 2001. Nonlinear finite-element modeling of batter piles under lateral load. J. Geotech. Geoenviron. Eng. 127 (7), 604–612.

Wang, Y.Z., He, L.L., 2013. Finite element analysis on bearing capacity of all-vertical-piled wharf in offshore deep-water. Ocean Eng. (Haiyang Gongcheng) 31 (6), 45–52, (in Chinese).

Wang, Y.Z., He, L.L., Wang, Z.Y., 2014. Research on dynamic simplified calculation method of all-vertical-piled wharf in offshore deep-water. Rock. Soil Mech. 35 (10), 2969–2976, (in Chinese).

Xie, Y.F., 1996. Behavior and bearing capacity of laterally loaded pile groups. Chin. J. Geotech. Eng. 18 (6), 39–45, (in Chinese).

Xie, Y.F., Liu, X.X., Tang, J.P., et al., 2015. Research on berthing capability and working property of pontoon bases. J. Coast. Res. 73, 505–510.

Zhu, D.T., Xie, Y.F., 2015. Hydrodynamic characteristics of offshore and pile breakwaters. Ocean Eng. 104, 257–265.